RESEARCH ARTICLE

INTERNATIONAL RESEARCH JOURNAL OF MULTIDISCIPLINARY TECHNOVATION

Asian Research Association

DOI: 10.54392/irjmt24310

Exploring Zinc Vanadate/Cobalt Oxide ($Zn_3(VO_4)_2$/CoO) Nano Hybrid Composites as Supercapacitors for Sustainable Energy Storage Applications

M. Gowtham [a], Chandrasekar Sivakumar [b], Narendhar Chandrasekar [c], S. Balachandran [d], N. Senthil Kumar [a,*]

[a] PG and Research and Department of Physics, Kongunadu Arts and Science College, Coimbatore 641029, Tamil Nadu, India

[b] Department of Physics, National Chung Hsing University, Taichung 40227, Taiwan

[c] Department of Bio Nano Technology, Gachon University, 1342, Seongnam-Daero, Sujeong-Gu, Seongnam 13120, Gyeonggi, Republic of Korea

[d] Department of Physiology, Saveetha Dental College and Hospital, Saveetha Institute of Medical and Technical Science, Saveetha University, Chennai 600077, Tamil Nadu, India

* Corresponding Author Email: kumarsrkvphy@gmail.com

DOI: https://doi.org/10.54392/irjmt24310

Received: 23-02-2024; Revised: 12-04-2024; Accepted: 20-04-2024; Published: 09-05-2024

Abstract: A hybrid nanocomposite of zinc vanadate/cobalt oxide ($Zn_3(VO_4)_2$/CoO at ratios of 90/10, 80/20, 50/50, and 20/80) was obtained using a simple co-precipitation technique, then calcinated for 4 hrs at 400°C. The surface morphological, vibrational, and structural characteristics of the synthesized hybrid nanocomposites were examined. According to the structural study, orthorhombic $Zn_3(VO_4)_2$ and cubic crystal systems of CoO with space groups Fm-3m were formed. The functional groups of Zinc Vanadate/Cobalt Oxide were examined using FTIR spectroscopy. A scanning electron microscopy (SEM) study reveals the nanosheets structures with the size of 200 nm. The chemical composition and formation of the $Zn_3(VO_4)_2$/CoO composites were confirmed using X-ray photoelectron spectroscopy (XPS). The electrochemical performance of the hybrid nanocomposites was assessed through CV, GCD and impedance analysis. Among the nanocomposites, $Zn_3(VO_4)_2$/CoO 80/20 exhibited a high specific capacitance value of 564.36 Fg^{-1} and retaining 97% of their total capacitance even after 3000 cycles.

Keywords: Zinc Vanadate, Cobalt Oxide, Supercapacitor, Energy storage applications

1. Introduction

Electrochemical reaction-based energy storage technologies have gained popularity due to their exceptional performance. Among these technologies, supercapacitors (SC) stand out as one of the most practical solutions for vehicles and as significant contributors to efficient power devices [1]. In comparison to traditional batteries and capacitors, supercapacitors provide higher power densities, improved rate capacities and better cycle stability [2, 3]. Pseudocapacitors and electric double-layer capacitors (EDLCs) are the two primary types of energy storage devices, which enhance the redox process by facilitating charge transfer across the electrode and electrolyte interfaces [4-7]. Supercapacitors, employ a range of electrode materials including carbon-based materials, conducting polymers, graphene, carbon spheres, and carbon nanotubes, alongside transition metal oxides such as ZnO, RuO_2, NiO, MnO_2, Co_3O_4, CuO, and Fe_2O_3 [8, 9]. However, the practical use of transition metal oxides (TMOs) is hindered by their relatively low specific capacitance. Of particular interest are mixed transition metal oxides, or MTMOs, which have emerged as promising low-cost materials for supercapacitors (SCs). MTMOs enable various redox reactions owing to the coexistence of two distinct metal species within a single crystal structure [10]. Similar to single TMOs, functional MTMOs can provide enhanced specific capacitance due to their broader potential window and increased number of electroactive sites [11-12].

Numerous nanostructures of vanadium oxide, including nanowires, nanobelts, and nanorods, have been investigated for potential application as electrode materials [13]. Vanadium oxide can be used as a metal cation to increase electrochemical productivity. In addition, they provide a host of benefits, including low cost, high operating stability, ease of setup, and environmental friendliness [14]. Their higher ionic conductivity and rapid proton mobility contribute to their lower internal resistance, rendering them desirable candidates [15]. Already the electrochemical behavior of a vanadium based-based mixed metal oxide compounds

were investigated using the hydrothermal method, revealing its high reversibility and an energy storage capacity [16-19].

Furthermore, a simple co-precipitation technique was employed to fabricate zinc vanadate nanoparticles, after being calcined at 600°C, it exhibited a specific capacitance of 312 F/g. [20]. It is surprising to discover that increasing the electrolyte operating voltage can elevate the overall functioning potential of the supercapacitor.

On the other hand, Liu et al. [21] recognized Co_3O_4 and CoO_x as potential electrode materials for supercapacitors owing to their intercalative pseudocapacitance characteristics. Lin et al. [22] achieved a maximum capacitance of 291 F/g by calcining CoOx xerogel at 150°C. Wang et al. [23] reported a single electrode capacitance of approximately 280 F/g for the $Co(OH)_2$ electrode, while Srinivasan and Weidner [24] observed capacitor-like behavior in the Co_3O_4 film used as a positive electrode. In supercapacitors Cobalt oxide electrodes have demonstrated excellent long-term performance, efficiency, and corrosion stability [25]. Consequently, the development of affordable, highly specialized surface area electroactive materials capable of undergoing reversible redox reactions remains a focal point of investigation for electrochemists.

Therefore, in view of the above facts, we opted to synthesize $Zn_3(VO_4)_2$.CoO using this method and investigated how varying scan speeds impacted the material's electrochemical performance. Additionally, we conducted a 3000-cycle stability analysis to assess its suitability for supercapacitor applications. Our findings indicate that the co-precipitation procedure provides a rapid and cost-effective means of producing consistent $Zn_3(VO_4)_2$.CoO nanocomposites.

2. Experimental section

To produce $Zn_3(VO_4)_2$.CoO nanocomposites, a co-precipitation method was employed. In a standard synthesis procedure, 0.089 mole of ammonium metavanadate (NH_4VO_3) and 0.40 mole of zinc acetate dihydrate $Zn(CH_3CO_2)_2{\cdot}2H_2O$ were separately dissolved in deionized water, labeled as solutions (1) and (2), respectively. These prepared solutions (1) and (2) were then combined and stirred continuously. To prepare a third solution, 0.44 moles of cobalt (II) acetate were dissolved in deionized water and constantly agitated (3). Upon adding the previously combined solutions (1) and (2) to solution (3), After adding ammonia solution to adjust the pH to 9, the mixture was continuously agitated at 80°C for six hours. The mixture was then left undisturbed overnight at room temperature to mature. The same process was repeated to create two composites with varying molar ratios of $Zn_3(VO_4)_2$/CoO (90/10, 80/20, 50/50, & 20/80). Centrifugation aided in separating the yellow precipitate formed from the remaining solution. The resulting powders were retained for further investigation and analysis after being dried at 60°C and then calcined at 400°C for four hours.

2.1 Electrode Preparation and Evolution

First, the Indium tin oxide (ITO) was cleaned using deionized water and subjected to ethanol sonication. Then ITO plates were left to air-dry naturally before being coated with Zinc vanadate copper oxide composites at a concentration of 7mg. The modified ITO plates were then baked overnight at 65°C to ensure thorough drying. Experimental procedures involved conducting electrochemical impedance spectroscopy, both differential pulse voltammetry, and cyclic voltammetry using a standard three-electrode cell configuration. This configuration consisted of an Ag/AgCl reference electrode, a platinum wire auxiliary electrode, and a 1 M KOH electrolyte solution. Electrochemical impedance spectroscopy employed an open circuit potential, a frequency range of 10^5-0.01 Hz, and an AC voltage amplitude of 5 mV. Galvanostatic charge/discharge tests were carried out using a Metrohm electrochemical workstation equipped with potentiostat-galvanostat capability, with current densities ranging from -0.1 to 0.5 V.

3. Result and Discussion

3.1 Structural and Morphological Analysis

Using XRD spectrum analysis, the structural properties of mixed phases of $Zn_3(VO_4)_2$/CoO (90/10, 80/20, 50/50, and 80/20) were investigated (Figure 1. (a-d)). With Zn occupying tetrahedral sites and V filling octahedral sites in the (Zn_8), zinc vanadate demonstrates orthorhombic spinel properties [26, 27]. Remarkably, the $Zn_3(VO_4)_2$/CoO composites exhibits highly intense diffraction peaks, indicating that the samples are crystalline in nature. Also, $Zn_3(VO_4)_2$ exhibits distinct and well-defined diffraction peaks at 2θ values of 24.41°, 29.17°, 33.15°, 43.58°, and 57.70° positioned and indexed as (200), (002), (022), (400), and (162) planes which match with the JCPDS no. 34–0378. While, diffraction peaks of cobalt oxide are observable at 2θ values of 42.61°, 61.84°, 74.10°, and 78.00°, corresponding to the (200), (220), (311), and (222) planes which match with the JCPDS no. 01-075–0418. As no impurities were detected, the zinc vanadate cobalt oxide composite exhibits exceptional purity. By applying the Debye-Scherrer formula, the crystallite sizes of zinc vanadate and cobalt oxide were determined. The resulting sizes were 134.26 nm and 45.47 nm, respectively (Table-1).

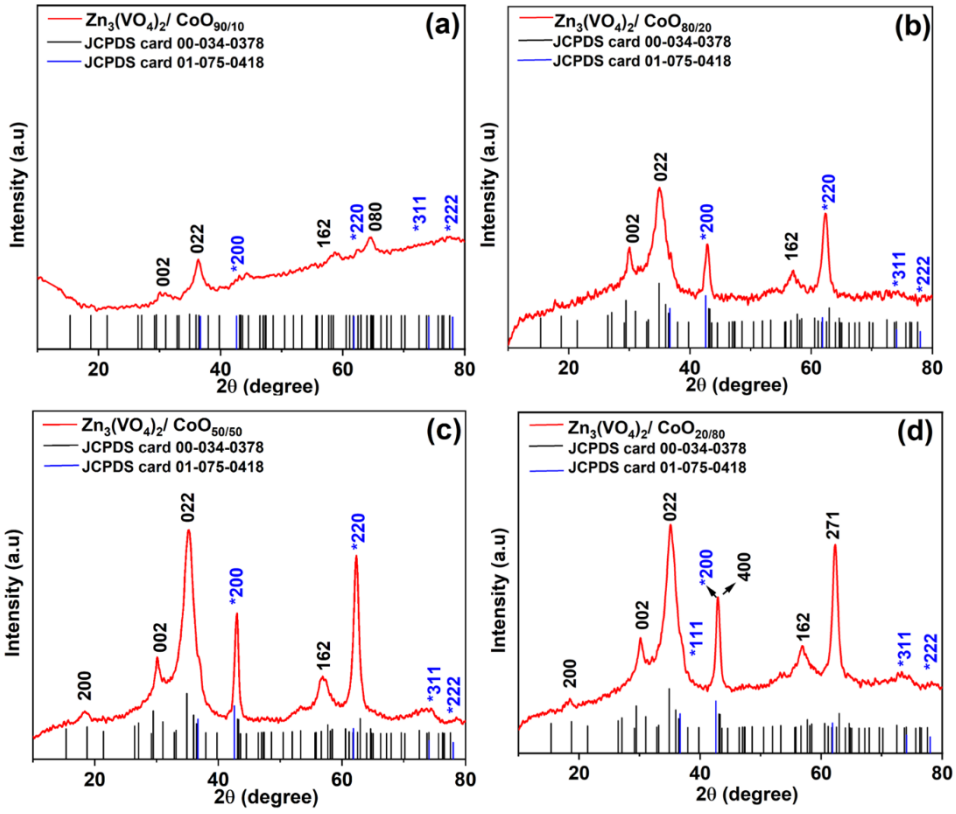

Figure 1. XRD spectrum of composites a) $Zn_3(VO_4)_2/CoO_{90/10}$ b) $Zn_3(VO_4)_2/CoO_{80/20}$, c) $Zn_3(VO_4)_2/CoO_{50/50}$, and d) $Zn_3(VO_4)_2/CoO_{20/80}$

Table 1. To the structural parameters of the calculate studied $Zn_3(VO_4)_2/CoO$ (90/10, 80/20, 50/50, and 80/20) nanocomposites samples

S.No.	Bragg angle 2 θ (deg)	FWHM value (deg)	(h k l) value			"D" Crystallite Size (nm)	"δ" dislocation X10^{14} (lines/ meter2)	"ε" strain X10^{4} (lin^{-2} met^{-4})	d spacing value (nm)
			h	k	l				
$Zn_3(VO_4)_2$	21.41	0.1695	2	0	0	49.86	4.02	7.27	4.15
	29.17	0.111	0	0	2	77.30	1.67	4.69	3.06
	33.153	0.0775	0	2	2	111.80	0.80	3.24	2.70
	57.705	0.1575	1	6	2	60.20	2.76	6.02	1.60
CoO	42.612	0.1695	2	0	0	52.59	3.62	6.89	2.12
	61.841	0.111	2	2	0	87.21	1.31	4.15	1.50
	74.105	0.0775	3	1	1	134.26	0.55	2.70	1.28

SEM examinations were conducted at various magnifications to analyze the structural morphology of the $Zn_3(VO_4)_2/CoO$ (90/10, 80/20, 50/50, and 80/20) composites, as depicted in Figure 2(a–d). SEM images vividly illustrate the flake-shaped morphology. The structure of interwoven growth in all directions is essential for the formation of the nano sheets.

EDS analysis of the prepared $Zn_3(VO_4)_2/CoO$ (90/10, 80/20, 50/50, and 80/20) is depicted in Figure 3, along with the elemental mapping spectrum (a–d).The EDS spectra of the prepared samples demonstrating that the produced nanocomposites solely contain components associated with Zn, V, Co, and O. Figure 3 illustrates the atomic and weight percentages of $Zn_3(VO_4)_2$, as well as the K ratio. The equal distribution of all four elements is discernible through mapping.

$Zn_3(VO_4)_2/CoO$ (90/10, 80/20, 50/50, and 80/20) composites exhibit distinctive features in their FTIR spectra (Figure-4). An evident absorption peak corresponding to water molecules and hydroxyl groups is noted in the wavenumber region of 3,600 to 3,000 cm^{-1}.

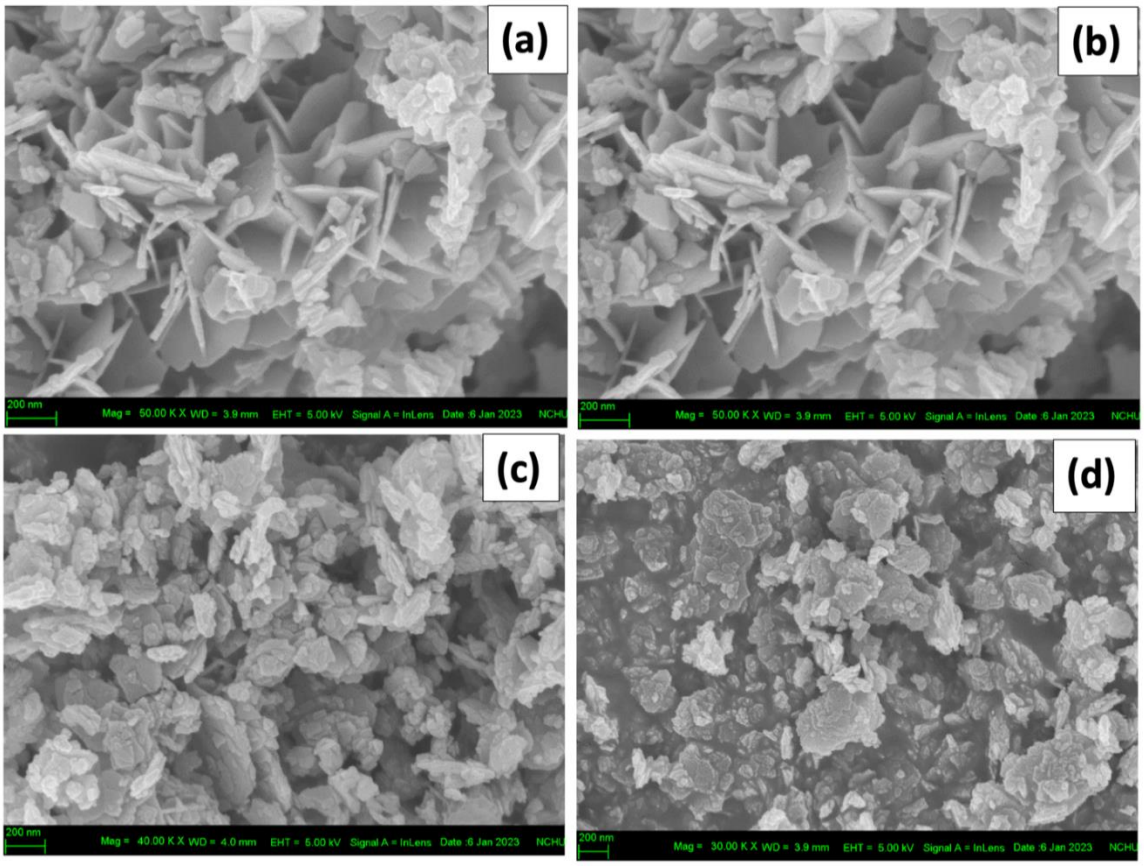

Figure 2. SEM images of the composites a) $Zn_3(VO_4)_2/CoO_{90/10}$ b) $Zn_3(VO_4)_2/CoO_{80/20}$, c) $Zn_3(VO_4)_2/CoO_{50/50}$, and d) $Zn_3(VO_4)_2/CoO_{20/80}$

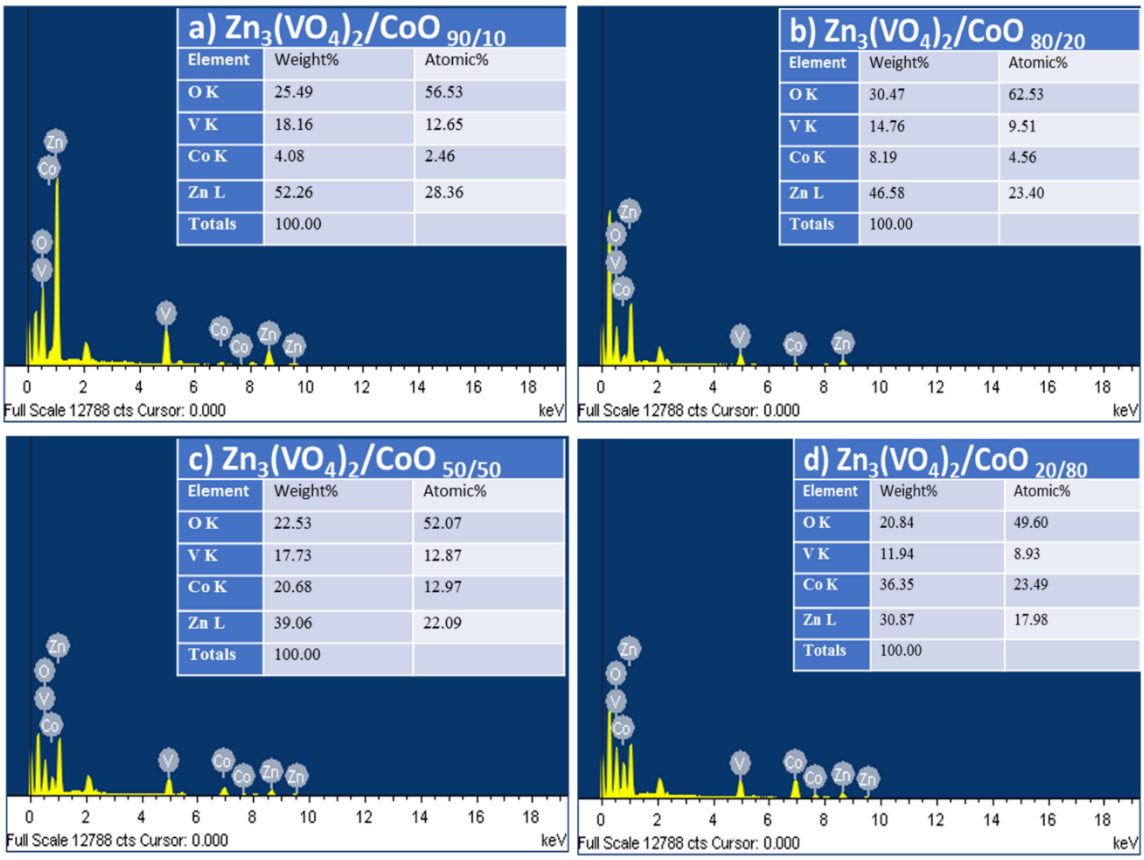

Figure 3. EDS Images of the Composites a) $Zn_3(VO_4)_2/CoO_{90/10}$ b) $Zn_3(VO_4)_2/CoO_{80/20}$, c) $Zn_3(VO_4)_2/CoO_{50/50}$, and d) $Zn_3(VO_4)_2/CoO_{20/80}$

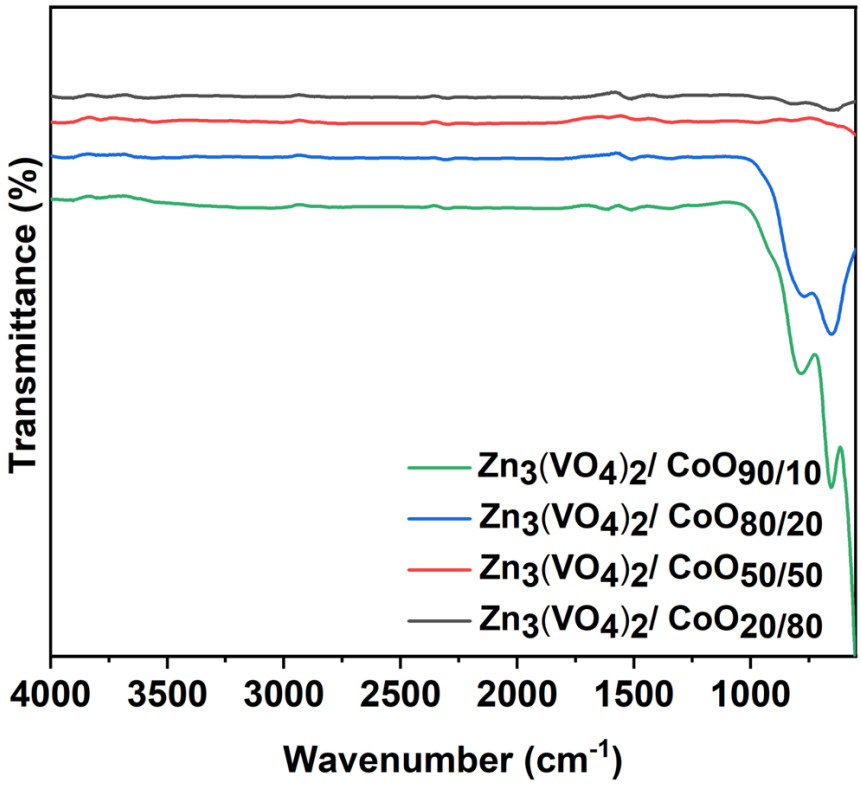

Figure 4. Fourier transforms infrared spectroscopy (FTIR) spectra of $Zn_3(VO_4)_2$/CoO composites

At 930 cm^{-1}, the vibrations of VO_4^{3-} and the V-O-Zn band manifest as peaks. Stretching modes of vanadate (V-O) are detected in the range of 925 to 935 cm^{-1}. The stretching vibrations of metal group V-O-V in the tetrahedral vibration of VO_4 are responsible for bands spanning from 650 to 780 cm^{-1}. Furthermore, the Zn-O, Zn-O-V, and Zn-O-Zn type extended modes of bonds are linked to the vibration band in the 770–650 cm^{-1} range. These modes originate from V = O linkages that are shared by the corner atoms of the tetrahedral structure (VO_4). Notable maxima of absorption at 567 and 661 cm^{-1} are observed in the cobalt oxide FTIR spectra.

The absorption band at 567 cm^{-1} represents the Co–O stretching vibration mode, while the absorption band at 661 cm^{-1} represents the O–Co–O bond bridging vibration [28, 29]. The FTIR spectrum's lack of additional peaks suggests the exceedingly pure nature of the treated material. However, peaks observed in the visible spectrum indicate that the chemical composition consists solely of metal oxide vanadate, a finding precisely confirmed by XRD analysis.

Figure 5(a) displays Zn, V, O, and Co, covering the entire analysis range. Peaks for Zn 2p3, Zn 2p1, V 2p3, V 2p, and Co 2p1 are observed at 1021.8, 1045.02, 517.3, 524.5, 530.1, 530.4, 780.1, and 796.2 eV, respectively. The core level spectra of the Zn 2p region in Figure 5(b) display two distinct peaks representing Zn $2p_{1/2}$ and Zn $2p_{3/2}$ of Zn^{2+} at 1045.02 eV and 1021.85 eV, respectively [30]. In Figure 5(c), the deconvoluted peaks of O 1s at 530.1 eV indicate lattice oxygen, while the peak at 531.4 eV is associated with absorbed oxygen species such as OH and H_2O on the surface of $Zn_3(VO_4)_2$/CoO. The V 2p XPS spectra in Figure 5(b) reveal distinctive peaks in two sections—$2p_{3/2}$ at 517.3 eV and $2p_{1/2}$ at 524.5 eV—with a spin-orbit splitting of 7.2 eV between them, indicating the presence of the V^{5+} state [31]. Deconvolution of the V 2p XPS peaks has facilitated a comprehensive analysis of vanadium oxidation states. The peak at 515.9 eV is attributed to the partial ionic reduction from +5 to +4 during the hydrothermal process [32]. An additional peak at 524.8 eV is assigned to V^{3+}. The broadening of the $V2p_{3/2}$ peak suggests a combination of V^{3+} and V^{5+} ion oxidation states [33]. Figure 5(d) presents a comparison of the cobalt 2p regions for various cobalt oxides. The measured cobalt binding energies for $2p_{1/2}$ and $2p_{3/2}$ were 795.7 eV and 779.8 eV, respectively. Additionally, two higher binding energies for CoO 2p, 780.5 and 796.6 eV, were identified.

3.2 Electrochemical analysis

The electrochemical performance of $Zn_3(VO_4)_2$/CoO composite materials (90/10, 80/20, 50/50, and 80/20) was evaluated using electrochemical impedance spectroscopy, charge-discharge analysis, and cyclic voltammetry. Cyclic voltammograms (CV) of the pure zinc vanadate electrode at scan rates ranging from 5 to 100 mV/s within the potential window of -1 to 1 V are depicted in Figure 6(a–e).

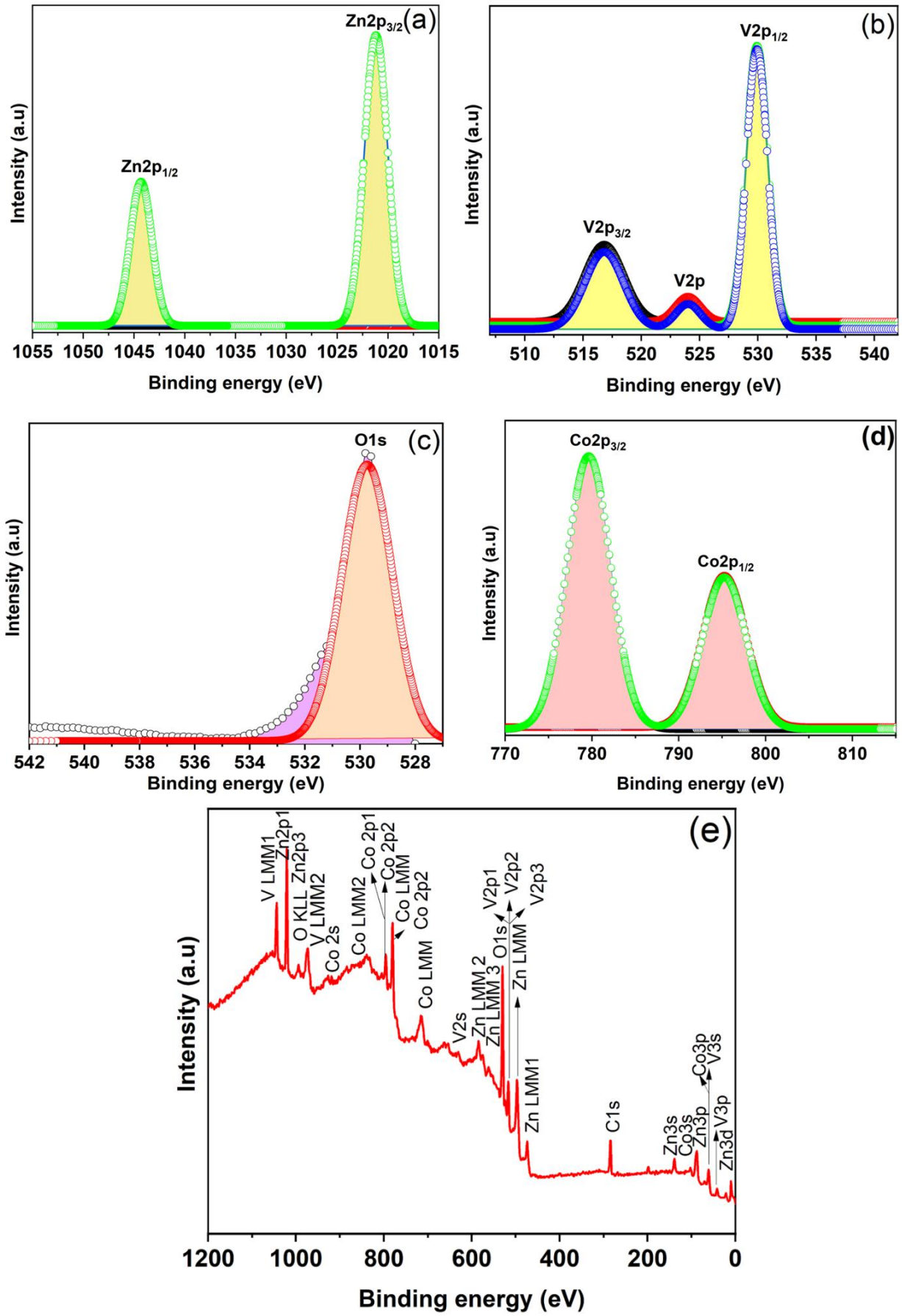

Figure 5. Xps Spectra of a) Zn 2p; b) V 2p; c) O1s; d) Co 2p energy regions; e) A wide range scan spectrum of $Zn_3(VO_4)_2/CoO_{20/80}$ composites

The cyclic voltammogram (CV) curves of the composite electrodes (80/20, 90/10, 50/50, and 80/20) comprising bare $Zn_3(VO_4)_2$/CoO are depicted in Figure 6a. These curves, exhibiting a rectangular shape with humps, indicate a combination of EDLC and Faradaic redox processes contributing to the capacitive responses [34-39]. Moreover, the evolution of the curve pattern along with increasing sweep rate underscores the significant role played by the hybrid nanocomposites in the electrode. Despite surface oxidation (Figure 6), the redox peaks in the $Zn_3(VO_4)_2$/CoO electrode remain subdued. The $Zn_3(VO_4)_2$/CoO composite electrode exhibits a broader CV curve area and more prominent anodic and cathodic peaks compared to the bare $Zn_3(VO_4)_2$ electrode.

The significant loop area observed on the CV curve of zinc vanadate composites confirms their enhanced capacity for charge storage. This improvement is attributed to the synergistic impact of $Zn_3(VO_4)_2$/CoO, which enhanced the composite's specific surface area and accelerates the transit of electrolyte ions, thereby exposing more electroactive sites to the KOH electrolyte. Wei et al. [40] reported similar behavior in electrodes exhibiting synergistic effects. $Zn_3(VO_4)_2$/CoO composites, responsible for enhancing the materials' wettability and introducing pseudocapacitance, are attributed to this phenomenon. [41].

Moreover, the distinct redox peaks provide evidence of the Faradic charge transfer experienced by the active material [42]. This indicates that, albeit subtly, K^+ ions are reversibly intercalated or deintercalated in the solid phase of $Zn_3(VO_4)_2$/CoO composites. Even at rapid scan rates of 20–100 mV/s, the redox peaks of the zinc vanadate composites remained easily discernible.

In this scenario, the ability of the $Zn_3(VO_4)_2$/CoO electrode to store charge stems from its interaction with protons or cations. Mobility of alkali cations in the electrolytes is crucial. Hydrated alkali K+ cations migrate from the KOH solution to the surface of the $Zn_3(VO_4)_2$/CoO electrode during negative potential scanning. They are absorbed onto the $Zn_3(VO_4)_2$/CoO surface upon arrival. Conversely, during the reverse scan, alkaline ions move back towards the electrolyte after desorption from the electrode [43].

Due to the extended sheet-like shape of the hybrid nanocomposite and the presence of active redox sites on the surface of $Zn_3(VO_4)_2$/CoO, there is a significant increase in electrolyte ion and electron accessibility. Redox reactions predominantly occur near these active areas. The movement of electrons and ions is facilitated by the grafted hybrid nanocomposite of $Zn_3(VO_4)_2$/CoO, contrasting with the bulkier $Zn_3(VO_4)_2$/CoO electrode (Fig. 6a). $Zn_3(VO_4)_2$/CoO nanocomposites enhances its conductivity and facilitates easy ion transit paths across the electrode. It's interesting to note that $Zn_3(VO_4)_2$ surfaces can increase the concentration of nano-sized voids and vacancies [44]. As a result, ions are able to access potentially larger active sites, as seen by the $Zn_3(VO_4)_2$ composite's CV curves.

In Figure 6a, the cathodic peak at -0.45 V is prominently visible and corresponds to the reduction of Zn^{2+} to metallic Zn. Additionally, the anodic signal at 0.5 V illustrates the oxidation of V^{2+} to V^{3+} and its subsequent interaction with Zn oxide to produce Zn^{2+} [45]. As voltage sweep rates increase from 5 to 100 mV/s, the anodic and cathodic peaks of $Zn_3(VO_4)_2$/CoO progressively shift towards positive and negative potentials, as depicted in Figure 6b. This phenomenon is attributed to the constant polarization effect observed in the $Zn_3(VO_4)_2$ combination (Figure 6c). Furthermore, it is indicated that K^+ ions exhibit limited effectiveness in intercalating the inner areas of the electrode's active zinc vanadate at higher current scan rates [46]. In these circumstances, the K^+ ions lack adequate time to permeate the extensive surface area of the active $Zn_3(VO_4)_2$ electrode material.

Consequently, with increasing scan rates, the redox peak intensifies [47]. Interestingly, the desolvation process is facilitated by the lower density of charge K^+ alkali ions, resulting in a slight deviation from ideal capacitive behavior in the CV curves of both electrodes.

Conversely, the unsynchronized movement of K^+ ions with current rates significantly reduces the specific capacitance of $Zn_3(VO_4)_2$/CoO at higher current rates [47]. The kinetic reversibility of Faradic redox reactions is indicated by the linear and symmetrical structure of the redox peaks [47, 48]. Furthermore, a slight fluctuation observed in the rectangular background of the CV curves suggests pseudocapacitive interactions between $Zn_3(VO_4)_2$/CoO and the electrolyte.

The capacitance retention capacity of these materials was examined through 3000 cyclic voltammetry (CV) cycles at a scan rate of 100 mV/s, as depicted in Figures 7(a-d).

The findings are summarized as follows: The specific capacitance (Csc) standards for $Zn_3(VO_4)_2$/CoO (90/10, 80/20, 50/50, & 80/20) electrodes were determined using equation (1).

$$Csc = \frac{\mathrm{Q}}{\mathrm{m}\Delta v} \qquad (1)$$

The mass of the electro-active material (m), the potential window (Δv), and the cathodic/anodic charges (Q) on each scan all contribute to the specific capacitance (Csc).

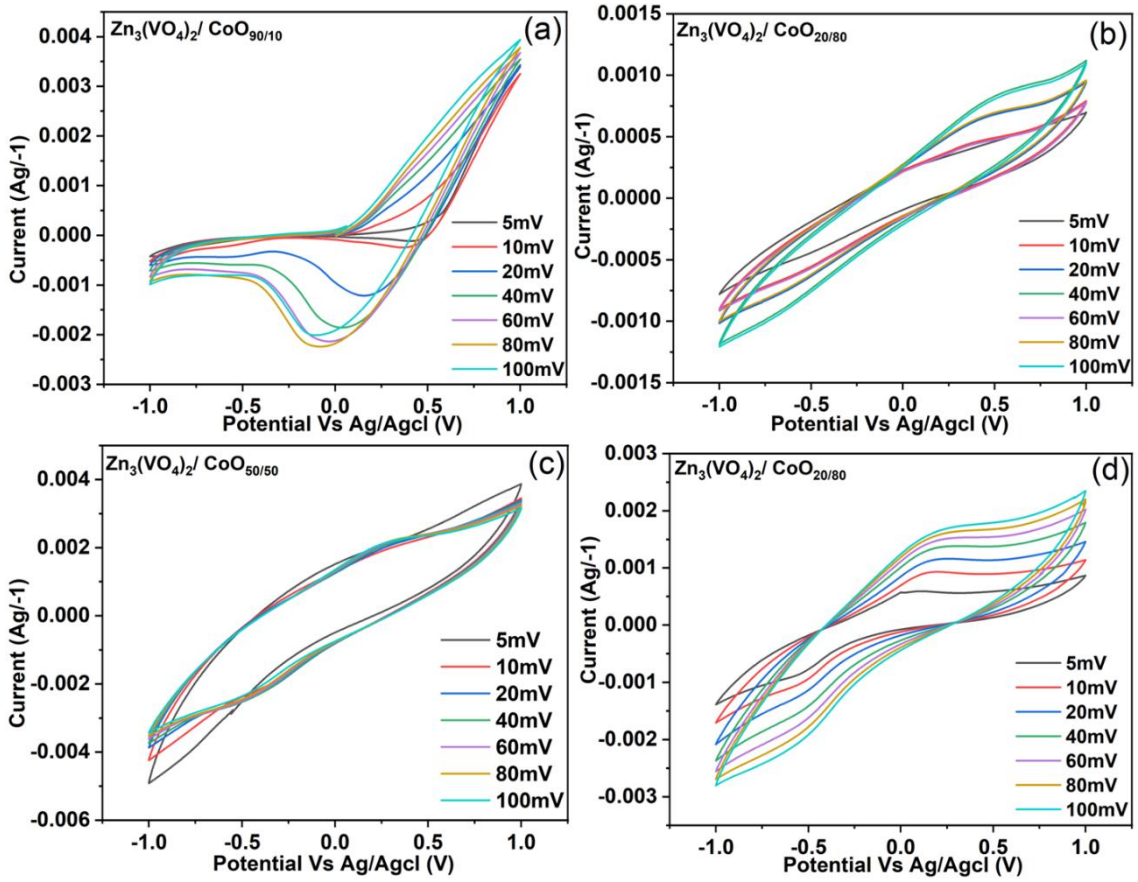

Figure 6. CV graphs of Zinc vanadate Cobalt oxide composites a) $Zn_3(VO_4)_2/CoO_{90/10}$ b) $Zn_3(VO_4)_2/CoO_{80/20}$, c) $Zn_3(VO_4)_2/CoO_{50/50}$, and d) $Zn_3(VO_4)_2/CoO_{20/80}$

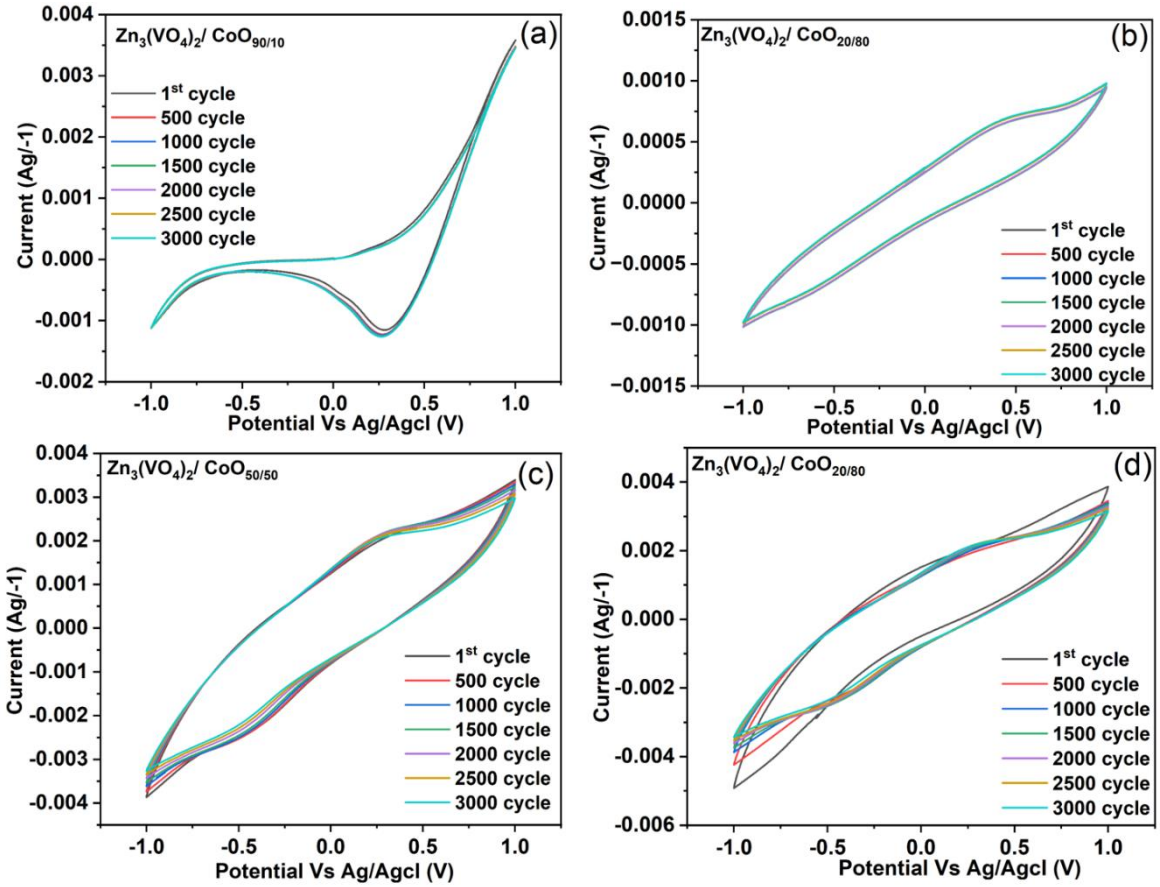

Figure 7. 3000 cycle of CV curve composites a) $Zn_3(VO_4)_2/CoO_{90/10}$ b) $Zn_3(VO_4)_2/CoO_{80/20}$, c) $Zn_3(VO_4)_2/CoO_{50/50}$, and d) $Zn_3(VO_4)_2/CoO_{20/80}$

Table 2. $Zn_3(VO_4)_2$/CoO composites specific capacitance value and percentage of retention

S.No	Percentage of nanocomposites (%)	Specific capacitance value (F g^{-1})	Percentage of retention (%)
1	$Zn_3(VO_4)_2$/CoO 90/10	153.86	95
2	$Zn_3(VO_4)_2$/CoO 80/20	234.30	95
3	$Zn_3(VO_4)_2$/CoO 50/50	549.23	97
4	$Zn_3(VO_4)_2$/CoO 20/80	564.36	97

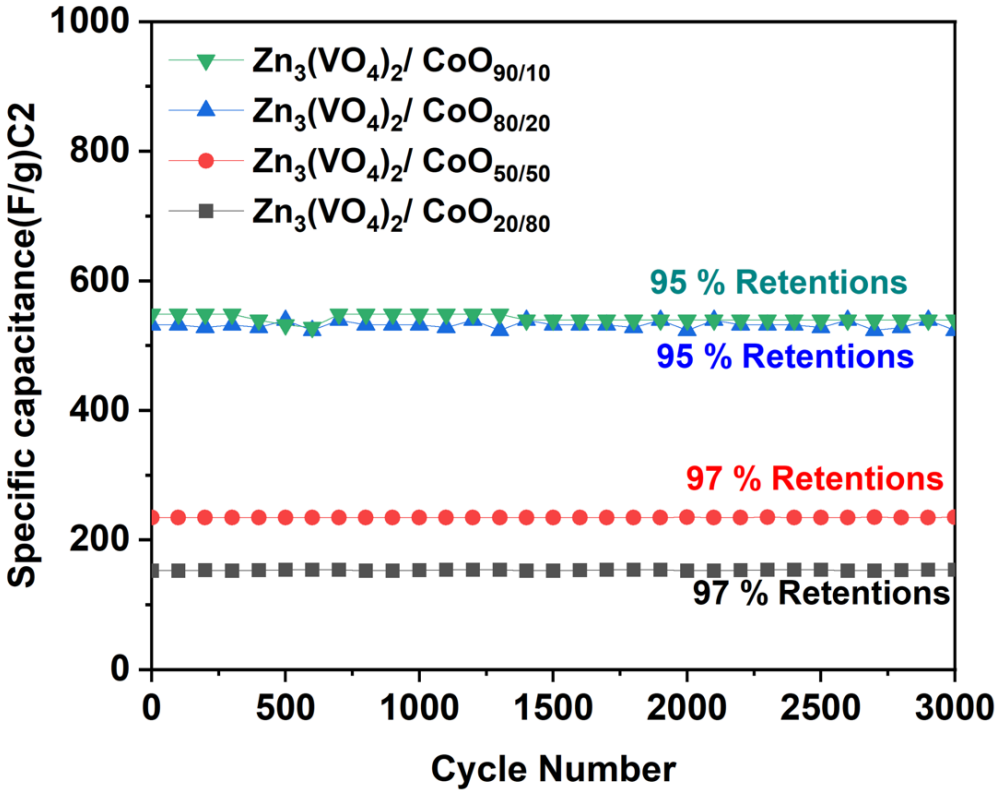

Figure 8. Specific capacitance Vs Cycle number retention graph

Table 2 summarizes the individual capacitance values and retention percentages of the manufactured samples after 3000 cycles. In Figure 8, the specific capacitance of the $Zn_3(VO_4)_2$/CoO (90/10, 80/20, 50/50, and 20/80) electrodes is illustrated. The $Zn_3(VO_4)_2$/CoO 90/10 composite displayed a specific capacitance value of 153.86 F/g with a retention rate of 95%. Similarly, the $Zn_3(VO_4)_2$/CoO 80/20 composite exhibited a specific capacitance value of 234.30 F/g with 95% retention. Demonstrating a specific capacitance value of 549.23 F/g with 97% retention, the $Zn_3(VO_4)_2$ 50/50 composite proved notable. Particularly noteworthy was the $Zn_3(VO_4)_2$ 20/80 composite, which achieved the highest specific capacitance value of 564.36 F/g with a retention rate of 97%, surpassing all other experiments. Figure 9 and Table 3 exhibits an comparative specific capacitance analysis.

Utilizing the appropriate chronopotentiometry technique, cycle testing at a constant current density allows for the investigation of specific capacitance and supercapacitive behavior in electrochemical storage devices. In Figure 10(a-d), the galvanostatic charge-discharge (GCD) curves of $Zn_3(VO_4)_2$ nanoparticles, covering potentials from 0 to 1 V and current densities ranging from 5 to 1 A/g, are presented. Chronopotentiometry is a technique that allows for the quantitative exploration of the anticipated supercapacitive characteristics of an electrode material by comparing cyclic voltammetry (CV) data. The non-linear discharge zone on the graph reflects the material's supercapacitive properties.

It was noted that there exists an inverse correlation between specific capacitance levels and current density. Elevated current densities during the redox process may lead to a reduction in electroactive material and an elevation in voltage drop, which could explain this phenomenon [57, 58]. The highest capacitance values were achieved at lower currents because ions could easily flow between the electrode surface and the active sites of the electrolyte. The characteristics necessary for a pseudocapacitive-type material are demonstrated by the inverse relationship between specific capacitance and current density [60, 61].

Table 3. $Zn_3(VO_4)_2$/CoO comparison of synthesis, electrode substrate, specific capacitance value, and electrolyte

Material	Synthesis method	Electrode coating substrate	Specific capacitance value	Electrolyte	Reference
$Zn_3(VO_4)_2$/CoO composites	Co-precipitation method	ITO plate	564.36 Fg^{-1}	KOH	Present work
Zinc vanadate	Co-precipitation method	nickel foil	312 Fg^{-1}	KOH	[20]
Zinc vanadate &N-MWNCT)	Hydrothermal method	Graphite Sheet	403 F g^{-1}	K_2SO_4	[18]
Zinc vanadate	Hydrothermal method	Graphite Sheet	383 F g^{-1}	KOH	[48]
Zinc Vanadate	Hydrothermal method	Graphite Sheet	213 F g^{-1}	K_2SO_4, Na_2SO_4 and KOH	[49]
Zinc Vanadate	Hydrothermal method	Ni-foam	427.7 F g^{-1}	KOH	[50]
Zinc Vanadate	Hydrothermal method	Ni-foam	302 F g^{-1}	KOH	[51]
Zinc Vanadate	Co-precipitation method	nickel foil	471 F g^{-1}	KOH	[52]
Zinc Vanadate	Hydrothermal method	Ni-foam	395 Fg^{-1}	K_2SO_4	[53]
α-Zinc Vanadate	Hydrothermal method	stainless steel	44.8 F g^{-1}	KCl	[54]
$Zn_3V_2O_8$− Ag@ C Composite	Rotational Chemical Bath Deposition	Metal substrate	380 F g^{-1}	KOH	[19]
Cobalt Oxide	SILAR method	copper substrates	165 F g^{-1}	KOH	[55]
Cobalt Oxide	Chemical synthesis	copper substrate	118 F g^{-1}	KOH	[56]
Cobalt Oxide	Hydrothermal method	Ni foam	278 F g^{-1}	KOH	[57]
Co_2O_3	Electrodeposition method	NiO substrate	345 F g^{-1}	KOH	[58]
rGO-cobalt oxide	Chemical synthesis	rGO nanosheets	276.1 F g^{-1}	KOH	[59]

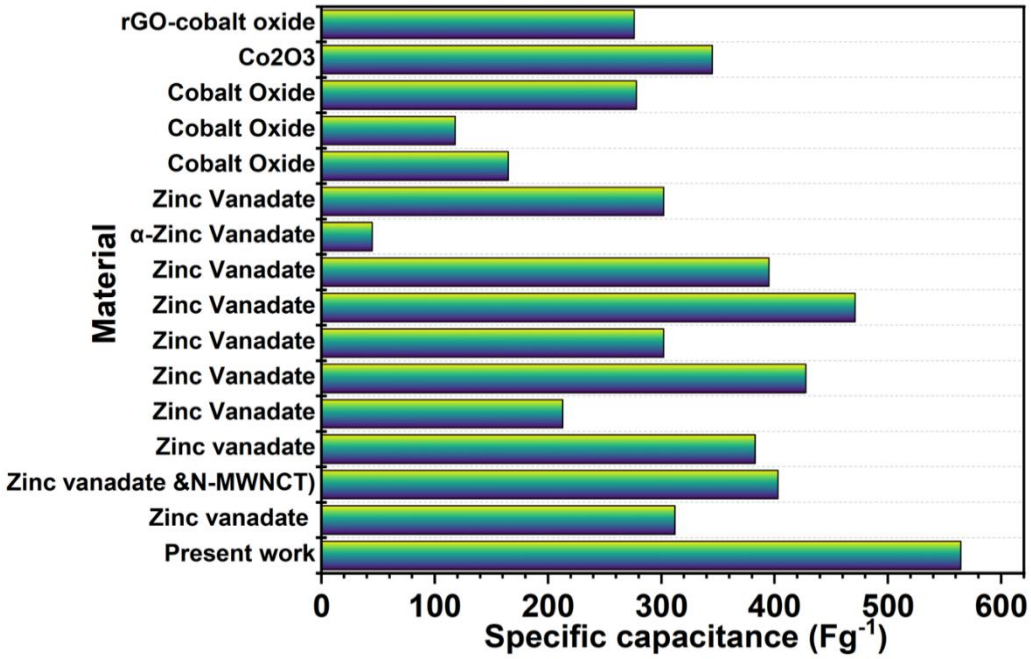

Figure 9. Comparison of specific capacitance graph

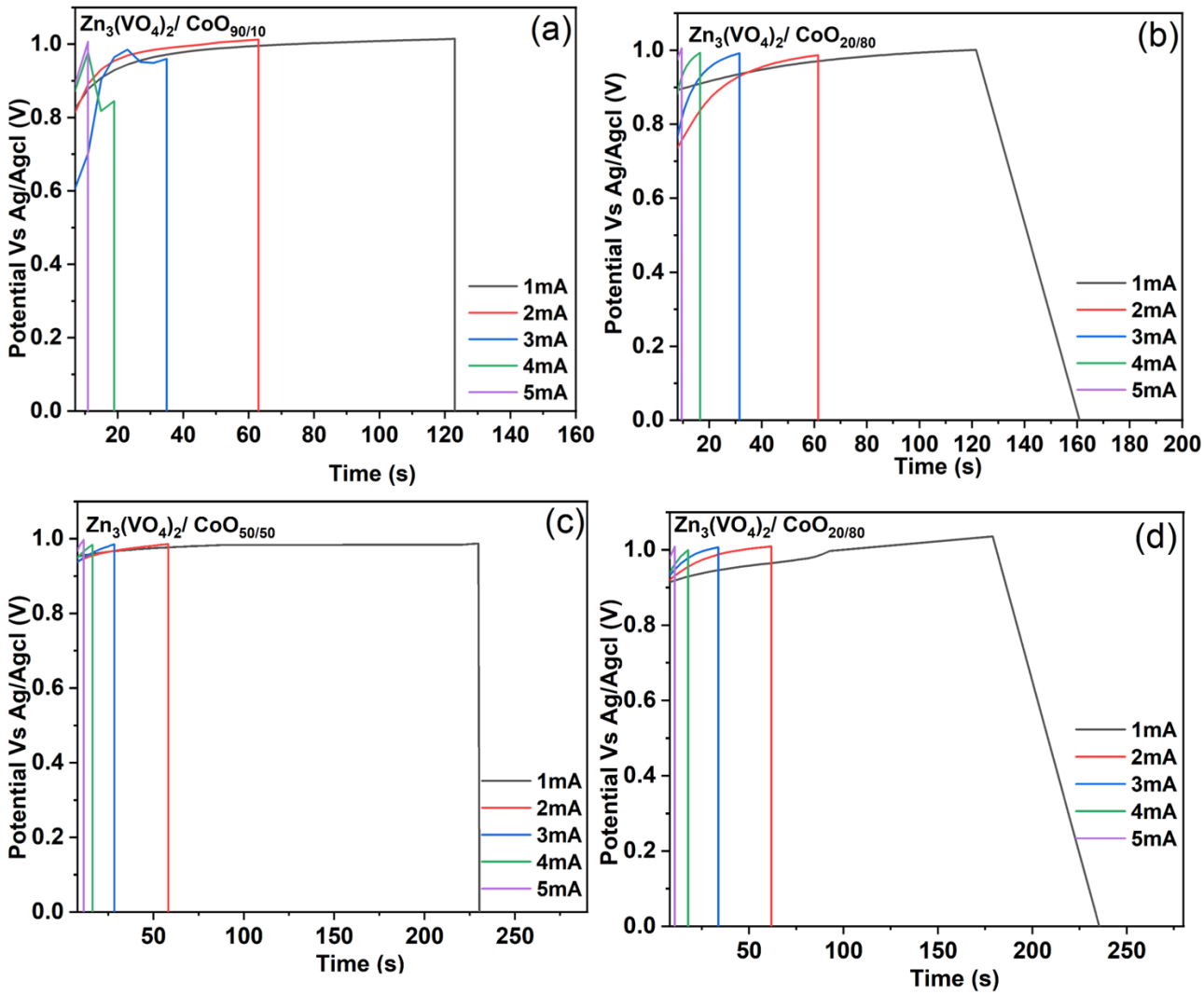

Figure 10. GCD curves of composites a) $Zn_3(VO_4)_2/CoO_{90/10}$ b) $Zn_3(VO_4)_2/CoO_{80/20}$, c) $Zn_3(VO_4)_2/CoO_{50/50}$, and d) $Zn_3(VO_4)_2/CoO_{20/80}$

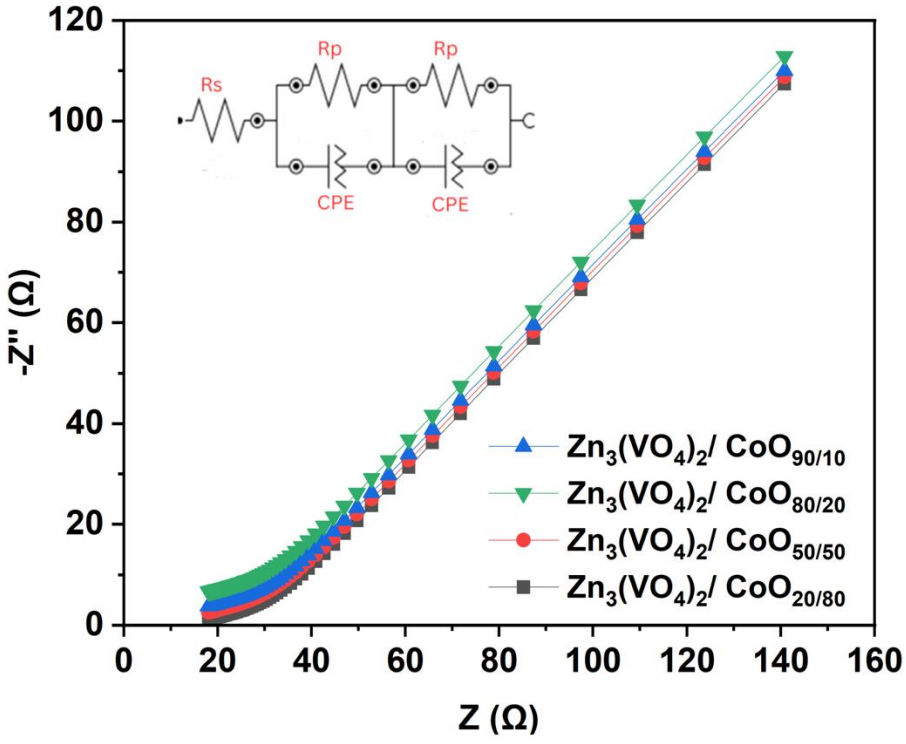

Figure 11. EIS spectra of $Zn_3(VO_4)_2/CoO$ composites

Electrochemical impedance measurements were conducted in the frequency range of 1 Hz to 100 kHz to explore the conductive and capacitive properties of the $Zn_3(VO_4)_2$ (90/10, 80/20, 50/50, and 80/20) materials in their assembled state.

The electrochemical impedance spectroscopy (EIS) patterns can be represented by a matching circuit, as depicted in the inset of Figure 11. These graphs can be divided into three sections: a linear segment in the low-frequency domain, correlating with the presence of electrolyte ions in the active material and the Warburg resistance, and a semicircular portion in the high-frequency range, representing the frequency-dependent diffusion of electrolyte ions [62]. The impedance curve of the $Zn_3(VO_4)_2$/CoO composites is depicted in Figure 11. showing a distorted semicircle in the high-frequency range and a linear trend in the low-frequency region. The equivalent series resistance (Rs), parallel resistance (Rp) of the electrode, and capacitance of the solid electrolyte interphase layer (CPE) are determined by the point where the semicircle intersects the real axis at high frequency. The diameter of the semicircle indicates the charge transfer resistance (Rct) of the $Zn_3(VO_4)_2$/CoO composites and the interface with the KOH electrolyte, while ionic diffusion is depicted by the vertical line in the low-frequency region (Warburg diffusion resistance).

4. Conclusion

In conclusion, a simple co-precipitation technique was employed successfully to produce a hybrid nanocomposite of zinc vanadate/cobalt oxide ($Zn_3(VO_4)_2$/CoO) at various ratios (90/10, 80/20, 50/50, and 20/80), followed by calcination at 400°C for four hours. Structural analysis revealed the formation of orthorhombic $Zn_3(VO_4)_2$ and cubic crystal systems of CoO with space groups Fm-3m, respectively. The presence of functional groups corresponding to $Zn_3(VO_4)_2$ and CoO was confirmed by FTIR spectroscopy. Scanning electron microscopy (SEM) investigations indicated formation of flake like nanosheets morphology. The surface chemistry of the $Zn_3(VO_4)_2$/CoO composites was examined utilizing X-ray photoelectron spectroscopy (XPS). Further, electrochemical performances such as cyclic voltammetry, charge-discharge analysis, and electrochemical impedance spectroscopy. After 3000 cycles, the $Zn_3(VO_4)_2$/CoO 80/20 nanocomposites exhibited a specific capacitance value of 564.36 F/g and a retention rate of 97%. These results suggest potential applications for the synthesized composites in sustainable energy storage and upcoming energy storage systems.

References

[1] C. Sengottaiyan, R. Jayavel, R.G. Shrestha, T. Subramani, S. Maji, J.H Kim, J.P.Hill, K. Ariga, and L. K. Shrestha, Indium oxide/carbon nanotube/reduced graphene oxide ternary nanocomposite with enhanced electrochemical supercapacitance. Bulletin of the Chemical Society of Japan, 92(3), (2019) 521-528. https://doi.org/10.1246/bcsj.20180338

[2] R. Kötz, M.J.E.A. Carlen, Principles and applications of electrochemical capacitors. Electrochimica acta, 45(15-16), (2000) 2483-2498. https://doi.org/10.1016/S0013-4686(00)00354-6

[3] N. Hassan, J. Riaz, M.T. Qureshi, A. Razaq, M. Rahim, A.M. Toufq, A. Shakoor, Vanadium oxide (V_2O_3) for energy storage applications through hydrothermal route. Journal of Materials Science: Materials in Electronics, 29, (2018) 16021-16026. https://doi.org/10.1007/s10854-018-9689-5

[4] S. Chaudhary, L.S. James, A.B.V. KiranKumar, C.H.V.V. Ramana, D.K. Mishra, S. Thomas, D. Kim, Reduced graphene oxide/ZnO nanorods nanocomposite: structural, electrical and electrochemical properties. Journal of Inorganic and Organometallic Polymers and Materials, 29, (2019) 2282-2290.https://doi.org/10.1007/s10904-019-01172-6

[5] L. L. Zhang, X. S. Zhao, Carbon-based materials as supercapacitor electrodes. Chemical society reviews, 38(9), (2009) 2520-2531. https://doi.org/10.1039/b813846j

[6] J. Liu, J. Wang, C. Xu, H. Jiang, C. Li, L. Zhang, J. Lin and Z.X. Shen, Advanced energy storage devices: basic principles, analytical methods, and rational materials design. Advanced science, 5(1), (2018) 1700322. https://doi.org/10.1002/advs.201700322

[7] A. Numan, Y. Zhan, M. Khalid and M. Hatamvand, Chapter three - introduction to supercapattery. Advances in Supercapacitor and Supercapattery, (2021) 45-61. https://doi.org/10.1016/B978-0-12-819897-1.00008-2

[8] M. Mayakannan, E. Vinoth, S. Prabakar. Synthesis and Structural, Optical Properties of Cadmium Doped Cobalt Oxide Nanoparticles. International Research Journal of Multidisciplinary Technovation. 3(3), (2021) 32-37. https://doi.org/10.34256/irjmt2135

[9] H Li, Y Liu, S Lin, H Li, Z Wu, L Zhu, C Li, X Wang, X Zhu, Y Sun, Laser crystallized sandwich-like MXene/Fe_3O_4/MXene thin film electrodes for flexible supercapacitors. Journal of Power Sources, 497, (2021) 229882. https://doi.org/10.1016/j.jpowsour.2021.229882

[10] W.H. Low, P.S. Khiew, S.S. Lim, C.W. Siong, E.R. Ezeigwe, Recent development of mixed transition metal oxide and graphene/mixed transition metal oxidebased hybrid nanostructures for advanced supercapacitors. Journal of Alloys and Compounds, 775, (2019) 1324-1356. https://doi.org/10.1016/j.jallcom.2018.10.102

[11] C.V.V.M. Gopi, R. Vinodh, S. Sambasivam, I.M. Obaidat, H.J. Kim, Recent progress of advanced energy storage materials for flexible and wearable supercapacitor: from design and development to applications. Journal of energy storage, 27, (2020) 101035. https://doi.org/10.1016/j.est.2019.101035

[12] B.O. Park, C.D. Lokhande, H.S. Park, K.D. Jung, K. D., O.S. Joo, Performance of supercapacitor with electrodeposited ruthenium oxide film electrodes-effect of film thickness. Journal of power sources, 134(1), (2004) 148-152. https://doi.org/10.1016/j.jpowsour.2004.02.027

[13] J. Yao, Y. Li, R.C. Massé, E. Uchaker, G. Cao. Revitalized interest in vanadium pentoxide as cathode material for lithium-ion batteries and beyond. Energy Storage Materials, 11, (2018) 205-259. https://doi.org/10.1016/j.ensm.2017.10.014

[14] K. Cao, T Jin, L. Yang, L. Jiao. Recent progress in conversion reaction metal oxide anodes for Li-ion batteries. Materials Chemistry Frontiers, 1(11), (2017) 2213-2242. https://doi.org/10.1039/C7QM00175D

[15] X. Zhang, C Jiang, J. Liang, W. Wu. Electrode materials and device architecture strategies for flexible supercapacitors in wearable energy storage. Journal of Materials Chemistry A, 9(13), (2021) 8099-8128. https://doi.org/10.1039/D0TA12299H

[16] W.H. Low, P.S. Khiew, S.S. Lim, C. W. Siong, E.R. Ezeigwe, Recent development of mixed transition metal oxide and graphene/mixed transition metal oxide based hybrid nanostructures for advanced supercapacitors. Journal of Alloys and Compounds, 775 (2019) 1324-1356. https://doi.org/10.1016/j.jallcom.2018.10.102

[17] L.N. Ramavathu, S.R. Harapanahalli, N. Pernapati, B.N. Tumma. Synthesis and characterization of Nickel Metavanadate ($Ni_3V_2O_8$) - application as photocatalyst and supercapacitor. International Journal of Nano Dimension, 12(4), (2021) 411-421.

[18] B. Suganya, S. Maruthamuthu, J. Chandrasekaran, B. Saravanakumar, E. Vijayakumar, R. Marnadu, Abdullah M. Al-Enizi, Mohd Ubaidullah, Design of zinc vanadate ($Zn_3V_2O_8$)/Nitrogen doped Multiwall Carbon Nanotubes (N-MWCNT) towards supercapacitor electrode applications. Journal of Electroanalytical Chemistry, 881, (2021) 114936. https://doi.org/10.1016/j.jelechem.2020.114936

[19] S.A. Mane, P.K. Bhoj, A.V. Moholkar, A. V. Ghule, (2024). Green and Facile Synthesis of $Zn_3V_2O_8$− Ag@ C Composite as an Efficient Electrode for Supercapacitor Application. ChemistrySelect, 9(9), (2024) e202305175. https://doi.org/10.1002/slct.202305175

[20] S.E. Arasi, P. Devendran, R. Ranjithkumar, S. Arunpandiyan, A. Arivarasan, Electrochemical property analysis of zinc vanadate nanostructure for efficient supercapacitors. Materials Science in Semiconductor Processing, 106, (2020) 104785. https://doi.org/10.1016/j.mssp.2019.104785

[21] T.C. Liu, W.G. Pell, B.E. Conway, Stages in the development of thick cobalt oxide films exhibiting reversible redox behavior and pseudocapacitance. Electrochimica acta, 44(17), (1999) 2829-2842. https://doi.org/10.1016/S0013-4686(99)00002-X

[22] C. Lin, J.A. Ritter, B.N. Popov, Characterization of sol-gel-derived cobalt oxide xerogels as electrochemical capacitors. Journal of the Electrochemical Society, 145(12), (1998) 4097. https://doi.org/10.1149/1.1838920

[23] X.F. Wang, Z. You, D.B. Ruan, A hybrid metal oxide supercapacitor in aqueous KOH electrolyte. Chinese Journal of Chemistry, 24(9), (2006) 1126-1132. https://doi.org/10.1002/cjoc.200690212

[24] V. Srinivasan, J.W. Weidner, Capacitance studies of cobalt oxide films formed via electrochemical precipitation. Journal of power sources, 108(1-2), (2002) 15-20. https://doi.org/10.1016/S0378-7753(01)01012-6

[25] H.K. Kim, T.Y. Seong, J.H. Lim, W.I. Cho, Y.S. Yoon, Electrochemical and structural properties of radio frequency sputtered cobalt oxide electrodes for thin-film supercapacitors. Journal of power sources, 102(1-2), (2001) 167-171. https://doi.org/10.1016/S0378-7753(01)00864-3

[26] J. Tang, S. Ni, B. Zhou, D. Chao, T. Li, X. Yang, Theoretical calculation and experimental verification of $Zn_3V_3O_8$ as an insertion type anode for LIBs, Journal of Alloys and Compounds, 730, (2018) 228-233. https://doi.org/10.1016/j.jallcom.2017.09.197

[27] M Wang, Y Shi and G Jiang. 3D hierarchical $Zn_3(OH)_2V_2O_7{\cdot}2H_2O$ and $Zn_3(VO_4)_2$ microspheres: Synthesis, characterization and

photoluminescence. Materials Research Bulletin, 47(1), (2012) 18-23.https://doi.org/10.1016/j.materresbull.2011.10.020

[28] L. Estepa, M. Daudon, Contribution of Fourier transform infrared spectroscopy to the identification of urinary stones and kidney crystal deposits. Biospectroscopy, 3(5), (1997) 347-369. https://doi.org/10.1002/(SICI)1520-6343(1997)3:5%3C347::AID-BSPY3%3E3.0.CO;2-%23

[29] S.H. Wu, D.H. Chen, Synthesis and characterization of nickel nanoparticles by hydrazine reduction in ethylene glycol. Journal of Colloid and Interface Science, 259(2), (2003) 282-286. https://doi.org/10.1016/S0021-9797(02)00135-2

[30] J. Bai, X. Li, G. Liu,Y. Qian, S. Xiong, Unusual formation of $ZnCo_2O_4$ 3D hierarchical twin microspheres as a high-rate and ultralong-life lithium-ion battery anode material. Advanced Functional Materials, 24(20), (2014) 3012-3020. https://doi.org/10.1002/adfm.201303442

[31] F.K. Butt, C. Cao, Q. Wan, P.Li, FaryalIdrees, M. Tahir, W.S. Khan, Z. Ali, M.J.M. Zapata, M. Safdar, X. Qub, Synthesis, evolution and hydrogen storage properties of ZnV_2O_4 glomerulus nano/microspheres: A prospective material for energy storage. International Journal of Hydrogen Energy, 39, (2014) 842−7851. https://doi.org/10.1016/j.ijhydene.2014.03.033

[32] S.D. Perera, B. Patel, N. Nijem, K. Roodenko, O. Seitz, J.P. Ferraris, Y.J. Chabal, K.J. Balkus Jr, Vanadium oxide nanowire–carbon nanotube binder-free flexible electrodes for supercapacitors. Advanced Energy Materials, 1(5), (2011) 936-945. https://doi.org/10.1002/aenm.201100221

[33] N.V. Hoa, T.T.H. Quyen, N.H. Nghia, N.V. Hieu, J.J. Shim, In situ growth of flower-like V2O5 arrays on graphene@nickel foam as high-performance electrode for supercapacitors. Journal of Alloys and Compounds, 702 (2017) 693-699. https://doi.org/10.1016/j.jallcom.2017.01.241

[34] J. Tang, R. R. Salunkhe, J. Liu, N. L. Torad, M. Imura, S. Furukawa, Y. Yamauchi, Thermal Conversion of Core-Shell Metal-Organic Frameworks: A New Method for Selectively Functionalized Nanoporous Hybrid Carbon. Journal of the American Chemical Society, 137 (2015) 1572- 1580. https://doi.org/10.1021/ja511539a

[35] W.H. Low, P.S. Khiew, S.S. Lim, C.W. Siong, C.H. Chia, E.R. Ezeigwe, Facile synthesis of graphene-Zn_3VO_8 nanocomposite as a high-performance electrode material for symmetric supercapacitor. Journal of Alloys and Compounds. 784, (2019) 847-858. https://doi.org/10.1016/j.jallcom.2019.01.137

[36] T.F. Qin, S.L. Peng, J.X. Hao, Y.X. Wen, Z.L. Wang, X.F. Wang, D.Y. He, J.C. Zhang, J. Hou, G.Z. Cao, Flexible and Wearable All-Solid-State Supercapacitors with Ultrahigh Energy Density Based on a Carbon Fiber Fabric Electrode. Advanced Energy Materials, 20 (2017) 1700409. https://doi.org/10.1002/aenm.201700409

[37] L. Niu, Y. Wang, F. Ruan, C. Shen, S. Shan, M. Xu, Z. Sun, C. Li, X. Liu, Y. Gong, In situ growth of $NiCo_2S_4$@$Ni_3V_2O_8$ on Ni foam as a binder-free electrode for asymmetric supercapacitors, All images. Journal of Materials Chemistry A, 4, (2016) 5669. https://doi.org/10.1039/C6TA00078A

[38] N. Choudhary, C. Li, J. Moore, N. Nagaiah, L. Zhai, Y. Jung, J. Thomas, Asymmetric Supercapacitor Electrodes and Devices. Advanced Materials, 29, (2017) 1605336. https://doi.org/10.1002/adma.201605336

[39] L. Wei, M. Sevilla, A. B. Fuertesc, R. Mokaya, G. Yushin, Hydrothermal carbonisation of abundant renewable natural organic chemicals for high-performance supercapacitor electrodes. Advanced Energy Materials, 1, (2011) 356-361. https://doi.org/10.1002/aenm.201100019

[40] Y. Yu, C. Niu, C. Han, K. Zhao, J. Meng, X. Xu, P. Zhang, L. Wang, Y. Wu, L. Mai, Zinc Pyrovanadate Nanoplates Embedded in Graphene Networks with Enhanced Electrochemical Performance. Industrial & Engineering Chemistry Research, 55, (2016) 2992-2999. https://doi.org/10.1021/acs.iecr.5b04811

[41] M. Dhananjaya, A. Lakshmi Narayana, N. Guru Prakash, P. Rosaiah, O.M. Hussain, intertwining network structured V_nO_{2n+1}-CNT/GO nanocomposite electrodes for supercapacitors. Materials Chemistry and Physics, 37, (2019) 121825. https://doi.org/10.1016/j.matchemphys.2019.121825

[42] S. Ramesh, S. Khandelwal, K.Y. Rhee, D. Hui, Synergistic effect of reduced graphene oxide, CNT and metal oxides on cellulose matrix for supercapacitor applications. Composites Part B: Engineering, 138, (2018) 45-54. https://doi.org/10.1016/j.compositesb.2017.11.024

[43] K. Thiagarajan, J. Theerthagiri, R.A. Senthil, P. Arunachalam, J. Madhavan, M. A. Ghanem,

Synthesis of $Ni_3V_2O_8$@graphene oxide nanocomposite as an efficient electrode material for supercapacitor applications. Journal of Solid-State Electrochemistry, 22, (2018) 527-536. https://doi.org/10.1007/s10008-017-3788-8

[44] P. He, M.Y. Yan, G.B. Zhang, R.M. Sun, L.N. Chen, Q.Y. An, L.Q. Mai, Layered VS2 nanosheet-based aqueous Zn ion battery cathode. Advanced Energy Materials, 11 (2017) 1601920. https://doi.org/10.1002/aenm.201601920

[45] M.S.M. Saleem, R. Swaminathan, V. Mohan, N. U. H. L. Ali, S.J. Kim, Sulfurization of cobalt oxide to cobalt sulfide: A positrode for the high-performance supercapacitor. Journal of Industrial and Engineering Chemistry, (2024). https://doi.org/10.1016/j.jiec.2024.02.038

[46] A. Chowdhury, R. Shukla, V. Sharma, S. Neogy, A. Chandra, V. Grover, A.K. Tyagi, controlling reaction kinetics of layered zinc vanadate having brucitelike ZneO layers supported by pyrovanadate pillars for use in supercapacitors. Journal of Alloys and Compounds, 829, (2020) 154479. https://doi.org/10.1016/j.jallcom.2020.154479

[47] B. Suganya, J. Chandrasekaran, S. Maruthamuthu, B. Saravanakumar, E. Vijayakumar, Hydrothermally Synthesized Zinc Vanadate Rods for Electrochemical Supercapacitance Analysis in Various Aqueous Electrolytes. Journal of Inorganic and Organometallic Polymers and Materials, 30, (2020) 4510-4519. https://doi.org/10.1007/s10904-020-01581-y

[48] Y. Li, Y. Teng, Z. Zhang, Y. Feng, P. Xue, W. Tonga, Xiaoyang Liu, Microwave-assisted Synthesized of Novel Nanostructured $Zn_3(OH)_2V_2O_7{\cdot}2H_2O$ and $Zn_2V_2O_7$ as Electrode Materials for Supercapacitors. New Journal of Chemistry, 41, (2017) 15298-15304. https://doi.org/10.1039/C7NJ03262E

[49] S. Vijayakumar, S-H. Lee, K-S. Ryu, Synthesis of $Zn_3V_2O_8$ nanoplatelets for lithium-ion battery and supercapacitor applications, RSC Advances, 5, (2015) 91822-91828. https://doi.org/10.1039/C5RA13904J

[50] S. Rajkumar, E. Elanthamilan, J. Princy Merlin, Facile Synthesis of $Zn_3V_2O_8$ Nanostructured material and its Enhanced Supercapacitive Performance. Journal of Alloys and Compounds, 861, (2021) 157939. https://doi.org/10.1016/j.jallcom.2020.157939

[51] B. Suganya, S. Maruthamuthu, J. Chandrasekaran, B. Saravanakumar, E. Vijayakumar, R. Marnadu, H. Elhosiny Ali, Tien Dai Nguyen, Nitrogen doped 2D graphene/$Zn_3V_2O_8$ nanocomposite with enhanced supercapacitive features, Surfaces and Interfaces, 24, (2021) 101129. https://doi.org/10.1016/j.surfin.2021.101129

[52] N. Venugopal, W-S. Kim, New α-$Zn_2V_2O_7$/carbon nanotube nanocomposite for supercapacitors, Korean Journal of Chemical Engineering volume 2015, 32, 1918-1923. https://doi.org/10.1007/s11814-014-0392-9

[53] S.G. Kandalkar, J.L. Gunjakar, C.D. Lokhande, Preparation of cobalt oxide thin films and its use in supercapacitor application. Applied Surface Science, 254(17), (2008) 5540-5544. https://doi.org/10.1016/j.apsusc.2008.02.163

[54] S.G. Kandalkar, D.S. Dhawale, C.K. Kim, C.D. Lokhande, Chemical synthesis of cobalt oxide thin film electrode for supercapacitor application. Synthetic Metals, 160(11-12), (2010) 1299-1302. https://doi.org/10.1016/j.synthmet.2010.04.003

[55] A. Numan, N. Duraisamy, F.S. Omar, Y.K. Mahipal, K. Ramesh, S. Ramesh, enhanced electrochemical performance of cobalt oxide nanocube intercalated reduced graphene oxide for supercapacitor application. RSC advances, 6(41), (2016) 34894-34902. https://doi.org/10.1039/C6RA00160B

[56] B. Sarma, R.S. Ray, S.K. Mohanty, M. Misra, Synergistic enhancement in the capacitance of nickel and cobalt based mixed oxide supercapacitor prepared by electrodeposition. Applied Surface Science, 300, (2014) 29-36. https://doi.org/10.1016/j.apsusc.2014.01.186

[57] R. Kumar, S. Sahoo, W.K. Tan, G. Kawamura, A. Matsuda, K.K. Kar, Microwave-assisted thin reduced graphene oxide-cobalt oxide nanoparticles as hybrids for electrode materials in supercapacitor. Journal of Energy Storage, 40, (2021) 102724. https://doi.org/10.1016/j.est.2021.102724

[58] R. Packiaraj, P. Devendran, S. Asath Bahadur, N. Nallamuthu, Structural and electrochemical studies of Scheelite type $BiVO_4$ nanoparticles: synthesis by simple hydrothermal method. Journal of Materials Science: Materials in Electronics, 29, (2018) 13265-13276, https://doi.org/10.1007/s10854-018-9450-0

[59] X. He, X. Zhang, A comprehensive review of supercapacitors: Properties, electrodes, electrolytes and thermal management systems based on phase change materials. Journal of energy storage, 56, (2022) 106023. https://doi.org/10.1016/j.est.2022.106023

[60] A. Shameem, P. Devendran, V. Siva, R. Packiaraj, N. Nallamuthu, S. Asath Bahadur, Electrochemical performance and optimization of α-$NiMoO_4$ by different facile synthetic approach for supercapacitor application. Journal of Materials Science: Materials in Electronics, 30 (2019) 3305-3315. https://doi.org/10.1007/s10854-018-00603-3

[61] Muktikanta Panigrahi, Investigation of Electrochemical Performance of PmAP/WO_3 Composite. International Research Journal of Multidisciplinary Technovation, 4(5) 2022 1-7. https://doi.org/10.54392/irjmt2251

[62] R. Muruganantham, I.V.B. Maggay, L.M.Z. De Juan, M.T. Nguyen, T. Yonezawa, C.-H. Lin, Y.-G. Lin, W.-R. Liu, Electrochemical exploration of the effects of calcination temperature of a mesoporous zinc vanadate anode material on the performance of Na-ion batteries, Inorganic Chemistry Frontiers, 6, (2019) 2653-2659. https://doi.org/10.1039/C9QI00494G

Authors Contribution Statement

M. Gowtham: Conceptualization, data curation, investigation, methodology, formal analysis, writing-original draft; Chandrasekar Sivakumar: formal analysis, writing-review and editing; Narendhar Chandrasekar: formal analysis, and writing-review; S. Balachandran: formal analysis, writing-review and editing; N. Senthilkumar: Conceptualization, Supervision, investigation, writing-original draft and editing. All authors have read and agreed to the published version of the manuscript.

Funding

The authors declares that no funds, grants, or other support were received during the preparation of this manuscript.

Competing Interests

The authors declares that there are no conflicts of interest regarding the publication of this manuscript.

Has this article screened for similarity?

Yes

About the License